Efficient solution of the electric and magnetic current combined-field integral equation with the multilevel fast multipole algorithm and block-diagonal preconditioning

Ö. Ergül[1,2] and L. Gürel[1,2]

Received 13 January 2009; revised 30 May 2009; accepted 18 June 2009; published 4 November 2009.

[1] We consider the efficient solution of electromagnetics problems involving dielectric and composite dielectric-metallic structures, formulated with the electric and magnetic current combined-field integral equation (JMCFIE). Dense matrix equations obtained from the discretization of JMCFIE with Rao-Wilton-Glisson functions are solved iteratively, where the matrix-vector multiplications are performed efficiently with the multilevel fast multipole algorithm. JMCFIE usually provides well conditioned matrix equations that are easy to solve iteratively. However, iteration counts and the efficiency of solutions depend on the contrast, i.e., the relative variation of electromagnetic parameters across dielectric interfaces. Owing to the numerical imbalance of off-diagonal matrix partitions, solutions of JMCFIE become difficult with increasing contrast. We present a four-partition block-diagonal preconditioner (4PBDP), which provides efficient solutions of JMCFIE by reducing the number of iterations significantly. 4PBDP is useful, especially when the contrast increases, and the standard block-diagonal preconditioner fails to provide a rapid convergence.

Citation: Ergül, Ö., and L. Gürel (2009), Efficient solution of the electric and magnetic current combined-field integral equation with the multilevel fast multipole algorithm and block-diagonal preconditioning, *Radio Sci.*, *44*, RS6001, doi:10.1029/2009RS004143.

1. Introduction

[2] For the solution of electromagnetics problems involving three-dimensional dielectric objects, the electric and magnetic current combined-field integral equation (JMCFIE) [*Ylä-Oijala and Taskinen*, 2005a, 2005b] is a preferable formulation in terms of accuracy and efficiency. In numerical solutions employing Rao-Wilton-Glisson (RWG) functions [*Rao et al.*, 1982] on triangles, JMCFIE is more accurate than the normal (N) formulations, such as the combined normal formulation (CNF) [*Ylä-Oijala et al.*, 2005b] and the modified normal Müller formulation (MNMF) [*Ylä-Oijala and Taskinen*, 2005b]. In addition, iterative solutions of problems involving large and complicated objects are more efficient with JMCFIE, which requires fewer iterations than MNMF and CNF [*Ergül and Gürel*, 2007, 2009]. For a given discretization with the RWG functions, the tangential (T) formulations, such as the combined tangential formulation (CTF) [*Ylä-Oijala et al.*, 2005b] and the Poggio-Miller-Chang-Harrington-Wu-Tsai (PMCHWT) formulation [*Poggio and Miller*, 1973; *Chang and Harrington*, 1977; *Wu and Tsai*, 1977], may provide more accurate results than JMCFIE. On the other hand, matrix equations obtained with the T formulations are difficult to solve iteratively [*Ylä-Oijala et al.*, 2005b, 2008; *Ergül and Gürel*, 2007, 2009]. In fact, improving the accuracy of JMCFIE solutions to the levels of the T formulations by refining the discretization can be more efficient than using the T formulations with coarse discretizations. Moreover, JMCFIE becomes essential for large problems, which might not easily be solved with the T formulations.

[3] JMCFIE can easily be applied to electromagnetics problems involving multiple dielectric regions or composite structures with coexisting metallic and dielectric parts [*Ylä-Oijala and Taskinen*, 2005a, 2005b; *Ylä-Oijala*, 2008]. In general, equivalent problems, which are defined

[1]Department of Electrical and Electronics Engineering, Bilkent University, Ankara, Turkey.
[2]Computational Electromagnetics Research Center, Bilkent University, Ankara, Turkey.

0048-6604/09/2009RS004143

for all nonmetallic regions, are discretized with oriented basis and testing functions. Then, the related unknowns on the boundaries and the corresponding equations are combined to form a single matrix equation to solve. This procedure is detailed by *Ylä-Oijala et al.* [2005a, 2005b] in the context of a PMCHWT formulation, and is extended to JMCFIE in the work of *Ylä-Oijala and Taskinen* [2005a, 2005b]. As discussed by *Ylä-Oijala and Taskinen* [2005a, 2005b], JMCFIE is appropriate for complicated structures involving multiple dielectric and metallic regions.

[4] Electromagnetics problems involving large metallic, dielectric, and composite objects can be solved iteratively, where the required matrix-vector multiplications are performed efficiently with the multilevel fast multipole algorithm (MLFMA) [*Song et al.*, 1997; *Sheng et al.*, 1998; *Chew et al.*, 2001; *Donepudi et al.*, 2003]. Recently, MLFMA is used to solve electromagnetics problems involving homogeneous dielectric objects formulated with JMCFIE [*Ergül and Gürel*, 2007, 2009]. In this study, we extend the MLFMA solution of JMCFIE to those problems involving multiple dielectric and composite dielectric-metallic structures. We mainly focus on the efficiency of the solutions and investigate the number of iterations for increasingly large objects. We show that iterative solutions of JMCFIE become difficult as the contrast increases, i.e., when electromagnetic parameters change significantly across dielectric interfaces. For efficient solutions of JMCFIE, we present a four-partition block-diagonal preconditioner (4PBDP), which reduces the iteration counts significantly. This preconditioner, which was originally developed by *Ergül and Gürel* [2009] for homogeneous dielectric objects, is particularly useful when a standard two-partition block-diagonal preconditioner (2PBDP) fails to provide a rapid convergence. In this paper, we present 4PBDP to accelerate the solution of more complicated problems involving multiple dielectric and metallic regions.

[5] The rest of the paper is organized as follows. Section 2 presents the matrix equations obtained with the JMCFIE formulation of electromagnetics problems involving multiple dielectric and metallic regions. MLFMA solutions are considered in section 3, where we provide the specific details of our implementation. Block-diagonal preconditioning is discussed in section 4, followed by numerical examples in section 5, and our concluding remarks in section 6. Time-harmonic electromagnetic fields with $e^{-i\omega t}$ time dependence are assumed throughout the paper.

2. Solutions of Electromagnetics Problems With JMCFIE

[6] We consider the general case involving U regions, namely, D_0, D_1,. . ., D_{U-1}, and D_0 is a region extending to infinity. Each region D_u for $u = 0, 1,. . ., (U - 1)$ is either metallic with perfect conductivity or lossless dielectric with constant electromagnetic parameters, i.e., permittivity ϵ_u and permeability μ_u. We assume that there is no junction where three or more regions intersect and each region D_u has a nonzero volume bounded by a closed surface S_u. Then,

$$S_u = \sum_{\substack{v=0 \\ v\neq u}}^{U-1} S_{uv}, \tag{1}$$

where $S_{uv} = S_{vu}$ is the interface between the regions D_u and D_v. We note that JMCFIE and MLFMA are also applicable to composite problems involving junctions and lossy dielectric regions [*Sheng et al.*, 1998; *Ylä-Oijala and Taskinen*, 2005a, 2005b].

[7] Applying the equivalence principle and using the boundary conditions for the tangential electric and magnetic fields on surfaces, equivalent electric and magnetic currents are defined as

$$\boldsymbol{J}(\boldsymbol{r}) = \hat{\boldsymbol{n}}(\boldsymbol{r}) \times \boldsymbol{H}(\boldsymbol{r}) \tag{2}$$

$$\boldsymbol{M}(\boldsymbol{r}) = -\hat{\boldsymbol{n}}(\boldsymbol{r}) \times \boldsymbol{E}(\boldsymbol{r}), \tag{3}$$

where $\hat{\boldsymbol{n}}(\boldsymbol{r})$ is the unit normal vector. For an interface S_{uv} for $u < v$, we choose $\hat{\boldsymbol{n}}$ directed into the region D_u. When S_{uv} is perfectly conducting, the tangential electric field and the magnetic current $\boldsymbol{M}(\boldsymbol{r})$ on the surface are zero.

2.1. Discretization

[8] For numerical solutions, surface currents are expanded in a series of RWG functions, i.e.,

$$\boldsymbol{J}(\boldsymbol{r}) = \sum_{n=1}^{N} a_n^J \boldsymbol{b}_n(\boldsymbol{r}) \tag{4}$$

$$\boldsymbol{M}(\boldsymbol{r}) = \sum_{n=1}^{N_D} a_n^M \boldsymbol{b}_n(\boldsymbol{r}), \tag{5}$$

where $\boldsymbol{b}_n(\boldsymbol{r})$ for $n = 1, 2,. . ., N$ represents the nth basis function with a spatial support of A_n, while a_n^J and a_n^M are the unknown coefficients. Since we assume that there is no junction, each RWG function is located on the interface of two regions, such as D_u and D_v. For $u < v$, D_u and D_v are called the "first" and "second" regions, respectively, of the RWG function. In addition, RWG functions are indexed by first considering the nonmetallic surfaces, which involve $N_D \leq N$ basis functions. On these surfaces, which separate two dielectric regions, both the electric and magnetic currents are expanded in a series of the same set of RWG functions $\boldsymbol{b}_n(\boldsymbol{r})$ for $n = 1, 2,. . ., N_D$. The remaining $(N - N_D)$ RWG functions, if any, are

defined on metallic surfaces to expand the electric current. Using a Galerkin scheme for the discretization, we employ the same set of RWG functions as the testing functions, i.e., there are N RWG functions to test the boundary conditions.

[9] In general, discretizations of JMCFIE lead to $(N + N_D) \times (N + N_D)$ dense matrix equations in the form of

$$\begin{bmatrix} \overline{\boldsymbol{Z}}^{(11)}_{N\times N} & \overline{\boldsymbol{Z}}^{(12)}_{N\times N_D} \\ \overline{\boldsymbol{Z}}^{(21)}_{N_D\times N} & \overline{\boldsymbol{Z}}^{(22)}_{N_D\times N_D} \end{bmatrix} \cdot \begin{bmatrix} \boldsymbol{a}^J \\ \boldsymbol{a}^M \end{bmatrix} = \begin{bmatrix} \boldsymbol{v}^{(1)} \\ \boldsymbol{v}^{(2)} \end{bmatrix}, \tag{6}$$

where

$$\boldsymbol{a}^J = \begin{bmatrix} a^J_1 & a^J_2 & \dots & a^J_N \end{bmatrix}^T \tag{7}$$

$$\boldsymbol{a}^M = \begin{bmatrix} a^M_1 & a^M_2 & \dots & a^M_{N_D} \end{bmatrix}^T \tag{8}$$

are column vectors involving the coefficients for the expansion of the electric and magnetic currents. Matrix elements and the elements of the right-hand side (RHS) vector are derived in the next sections.

2.2. Matrix Elements

[10] Consider the interaction between a basis function $\boldsymbol{b}_n(\boldsymbol{r})$ and a testing function $\boldsymbol{t}_m(\boldsymbol{r})$, and let a dielectric region D_u be common for the two functions. Then, the corresponding matrix element in the diagonal partition $\overline{\boldsymbol{Z}}^{(11)}$ in (6) can be written as

$$\begin{aligned} Z^{(11)}_{mn} \xleftarrow{+} & -\frac{\gamma_n\gamma_m}{2}\int_{A_m} d\boldsymbol{r}\boldsymbol{t}_m(\boldsymbol{r})\cdot\boldsymbol{b}_n(\boldsymbol{r}) \\ & + \gamma_n \int_{A_m} d\boldsymbol{r}\boldsymbol{t}_m(\boldsymbol{r})\cdot\hat{\boldsymbol{n}}(\boldsymbol{r})\times\boldsymbol{\mathcal{K}}_u\{\boldsymbol{b}_n\}(\boldsymbol{r}) \\ & + \gamma_n\gamma_m \int_{A_m} d\boldsymbol{r}\boldsymbol{t}_m(\boldsymbol{r})\cdot\boldsymbol{\mathcal{T}}_u\{\boldsymbol{b}_n\}(\boldsymbol{r}), \end{aligned} \tag{9}$$

where we use the "$\xleftarrow{+}$" notation to indicate the "cumulative addition operation," since the value in (9) may not be the only contribution to $Z^{(11)}_{mn}$. Specifically, if $\boldsymbol{t}_m(\boldsymbol{r})$ and $\boldsymbol{b}_n(\boldsymbol{r})$ are on the same nonmetallic surface, both regions of these functions are common, and the corresponding matrix element $Z^{(11)}_{mn}$ involves two sets of contributions, i.e., interactions of the basis and testing functions through the two regions.

[11] In (9), the integro-differential operators $\boldsymbol{\mathcal{T}}_u$ and $\boldsymbol{\mathcal{K}}_u$ for region D_u are applied on the basis function, i.e.,

$$\begin{aligned} \boldsymbol{\mathcal{T}}_u\{\boldsymbol{b}_n\}(\boldsymbol{r}) = & ik_u\int_{A_n} d\boldsymbol{r}'\boldsymbol{b}_n(\boldsymbol{r}')g_u(\boldsymbol{r},\boldsymbol{r}') \\ & + \frac{i}{k_u}\int_{A_n} d\boldsymbol{r}'\nabla'\cdot\boldsymbol{b}_n(\boldsymbol{r}')\nabla g_u(\boldsymbol{r},\boldsymbol{r}') \end{aligned} \tag{10}$$

$$\boldsymbol{\mathcal{K}}_u\{\boldsymbol{b}_n\}(\boldsymbol{r}) = \int_{PV,A_n} d\boldsymbol{r}'\boldsymbol{b}_n(\boldsymbol{r}')\times\nabla' g_u(\boldsymbol{r},\boldsymbol{r}'), \tag{11}$$

where PV indicates the principal value of the integral, $k_u = \omega\sqrt{\epsilon_u\mu_u}$ is the wave number, and

$$g_u(\boldsymbol{r},\boldsymbol{r}') = \frac{\exp(ik_uR)}{4\pi R} \qquad (R = |\boldsymbol{r}-\boldsymbol{r}'|) \tag{12}$$

denotes the homogeneous-space Green's function. Using a Galerkin scheme, both $\boldsymbol{\mathcal{K}}_u$ and $\boldsymbol{\mathcal{T}}_u$ operators are well tested in the diagonal partitions of JMCFIE [*Ylä-Oijala and Taskinen*, 2005a, 2005b; *Ylä-Oijala et al.*, 2005b]. In (9), the signs $\gamma_m = \pm 1$ and $\gamma_n = \pm 1$ are determined by the orientation of the basis and testing functions. If the common region D_u is the "first" region for the basis (testing) function, then $\gamma_n = +1$ ($\gamma_m = +1$); otherwise, $\gamma_n = -1$ ($\gamma_m = -1$).

[12] When the basis function $\boldsymbol{b}_n(\boldsymbol{r})$ is not on a metallic surface, i.e., $n \le N_D$, there exists a matrix element $Z^{(12)}_{mn}$ in (6). A contribution to this element due to the interaction of the basis and testing functions through the common region D_u can be written as

$$\begin{aligned} Z^{(12)}_{mn} \xleftarrow{+} & -\frac{\gamma_n}{2}\eta_u^{-1}\int_{A_m} d\boldsymbol{r}\boldsymbol{t}_m(\boldsymbol{r})\cdot\hat{\boldsymbol{n}}(\boldsymbol{r})\times\boldsymbol{b}_n(\boldsymbol{r}) \\ & + \gamma_n\eta_u^{-1}\int_{A_m} d\boldsymbol{r}\boldsymbol{t}_m(\boldsymbol{r})\cdot\hat{\boldsymbol{n}}(\boldsymbol{r})\times\boldsymbol{\mathcal{T}}_u\{\boldsymbol{b}_n\}(\boldsymbol{r}) \\ & - \gamma_n\gamma_m\eta_u^{-1}\int_{A_m} d\boldsymbol{r}\boldsymbol{t}_m(\boldsymbol{r})\cdot\boldsymbol{\mathcal{K}}_u\{\boldsymbol{b}_n\}(\boldsymbol{r}), \end{aligned} \tag{13}$$

where η_u is the impedance of the region. As opposed to the diagonal partitions, $\boldsymbol{\mathcal{K}}_u$ and $\boldsymbol{\mathcal{T}}_u$ operators are weakly tested in (13) using a Galerkin scheme. When the testing function $\boldsymbol{t}_m(\boldsymbol{r})$ is not on a metallic surface, i.e., $m \le N_D$, there exists a matrix element $Z^{(21)}_{mn}$ with a contribution as

$$\begin{aligned} Z^{(12)}_{mn} \xleftarrow{+} & \frac{\gamma_n}{2}\eta_u\int_{A_m} d\boldsymbol{r}\boldsymbol{t}_m(\boldsymbol{r})\cdot\hat{\boldsymbol{n}}(\boldsymbol{r})\times\boldsymbol{b}_n(\boldsymbol{r}) \\ & - \gamma_n\eta_u\int_{A_m} d\boldsymbol{r}\boldsymbol{t}_m(\boldsymbol{r})\cdot\hat{\boldsymbol{n}}(\boldsymbol{r})\times\boldsymbol{\mathcal{T}}_u\{\boldsymbol{b}_n\}(\boldsymbol{r}) \\ & + \gamma_n\gamma_m\eta_u\int_{A_m} d\boldsymbol{r}\boldsymbol{t}_m(\boldsymbol{r})\cdot\boldsymbol{\mathcal{K}}_u\{\boldsymbol{b}_n\}(\boldsymbol{r}). \end{aligned} \tag{14}$$

Finally, when both basis and testing functions are not on metallic surfaces, there exists a matrix element $Z^{(22)}_{mn}$, which is equal to the corresponding element of $\overline{\boldsymbol{Z}}^{(11)}$, i.e.,

$$Z^{(22)}_{mn} = Z^{(11)}_{mn}, \tag{15}$$

for $m \le N_D$ and $n \le N_D$. If a structure does not involve any metallic surfaces, the diagonal partitions of the matrix equations obtained with JMCFIE are identical.

This is a desirable property in terms of conditioning and iterative convergence [*Ylä-Oijala et al.*, 2005b].

2.3. RHS Vector

[13] The RHS vector in (6) is obtained by testing the incident electromagnetic fields. In general, each nonmetallic region may host some external sources that produce incident electric and magnetic fields, i.e., $\boldsymbol{E}_u^{inc}(\boldsymbol{r})$ and $\boldsymbol{H}_u^{inc}(\boldsymbol{r})$. Consider an RWG function $\boldsymbol{t}_m(\boldsymbol{r})$ on the surface of a nonmetallic region D_u. The incident fields in D_u are tested by $\boldsymbol{t}_m(\boldsymbol{r})$ and added to the related element in the upper partition of the RHS vector, i.e.,

$$v_m^{(1)} \xleftarrow{+} -\gamma_m \int_{A_m} d\boldsymbol{r} \boldsymbol{t}_m(\boldsymbol{r}) \cdot \hat{\boldsymbol{n}}(\boldsymbol{r}) \times \boldsymbol{H}_u^{inc}(\boldsymbol{r}) - \gamma_m \eta_u^{-1} \int_{A_m} d\boldsymbol{r} \boldsymbol{t}_m(\boldsymbol{r}) \cdot \boldsymbol{E}_u^{inc}(\boldsymbol{r}), \quad (16)$$

where $\gamma_m = \pm 1$ is determined by the orientation of $\boldsymbol{t}_m(\boldsymbol{r})$. In addition, when the testing function $\boldsymbol{t}_m(\boldsymbol{r})$ is not on a metallic surface, i.e., $m < N_D$, there exists a corresponding element in the second partition of the RHS vector in (6). Contribution to this element due to the incident fields in region D_u can be written as

$$v_m^{(2)} \xleftarrow{+} \gamma_m \int_{A_m} d\boldsymbol{r} \boldsymbol{t}_m(\boldsymbol{r}) \cdot \hat{\boldsymbol{n}}(\boldsymbol{r}) \times \boldsymbol{E}_u^{inc}(\boldsymbol{r}) - \gamma_m \eta_u \int_{A_m} d\boldsymbol{r} \boldsymbol{t}_m(\boldsymbol{r}) \cdot \boldsymbol{H}_u^{inc}(\boldsymbol{r}). \quad (17)$$

3. MLFMA Solutions of Electromagnetics Problems Formulated With JMCFIE

[14] Matrix equations obtained with JMCFIE can be solved iteratively by employing a Krylov subspace algorithm, where the required matrix-vector multiplications are performed efficiently with MLFMA in $\mathcal{O}(N \log N)$ time using $\mathcal{O}(N \log N)$ memory [*Song et al.*, 1997]. A multilevel tree structure with $\mathcal{O}(\log N)$ levels is constructed by placing the object in a cubic box and recursively dividing the computational domain into subdomains (clusters). Then, interactions of the basis and testing functions that are far from each other can be calculated approximately and efficiently in a group-by-group manner. In general, each matrix-vector multiplication performed by MLFMA involves three main stages called aggregation, translation, and disaggregation. These stages, which are performed on the multilevel tree structure, can be summarized as follows:

[15] 1. The first stage is aggregation. Radiated fields of clusters are calculated from the bottom of the tree structure to the highest level. In the lowest level, the radiated field of a cluster is obtained by combining the radiation patterns of the basis functions inside the cluster. In the upper levels, the radiated field of a cluster is the combination of the radiated fields of its subclusters.

[16] 2. The second stage is translation. Radiated fields computed during the aggregation stage are translated into incoming fields. For each cluster at any level, there are $\mathcal{O}(1)$ clusters to translate the radiated field to.

[17] 3. The third stage is disaggregation. Total incoming fields at cluster centers are calculated from the top of the tree structure to the lowest level. The total incoming field for a cluster is obtained by combining incoming fields due to translations and the incoming field to the center of its parent cluster, if it exists. In the lowest level, incoming fields are received by testing functions.

[18] MLFMA is investigated extensively in various references [e.g., *Song et al.*, 1997; *Sheng et al.*, 1998; *Chew et al.*, 2001; *Donepudi et al.*, 2003]. In this paper, we provide only the specific details of our implementation.

[19] 1. For a general problem involving U regions, MLFMA must be applied for each nonmetallic region separately [*Donepudi et al.*, 2003; *Luo and Lu*, 2007; *Fostier and Olyslager*, 2008]. This is because the Green's function depends on the electromagnetic parameters of the region, i.e., ϵ_u and μ_u. In addition, radiated and incoming fields of clusters are defined and sampled on the unit sphere, and the number of samples depends on the cluster size as measured by the wavelength [*Koc et al.*, 1999]. Hence, the sampling rate and the resulting tree structure also depend on the electromagnetic parameters of the region.

[20] 2. For each region D_u, we perform four matrix-vector multiplications with the four partitions of the system matrix, i.e.,

$$\boldsymbol{y}^{(1)} = \overline{\boldsymbol{Z}}_u^{(11)} \cdot \boldsymbol{x}^{\boldsymbol{J}} + \overline{\boldsymbol{Z}}_u^{(12)} \cdot \boldsymbol{x}^{\boldsymbol{M}} \quad (18)$$

$$\boldsymbol{y}^{(2)} = \overline{\boldsymbol{Z}}_u^{(21)} \cdot \boldsymbol{x}^{\boldsymbol{J}} + \overline{\boldsymbol{Z}}_u^{(22)} \cdot \boldsymbol{x}^{\boldsymbol{M}}, \quad (19)$$

where the coefficients $\boldsymbol{x}^{\boldsymbol{J}}$ and $\boldsymbol{x}^{\boldsymbol{M}}$ are provided by the iterative algorithm. We note that a set of aggregation, translation, and disaggregation stages is performed once for a multiplication with a partition, although each partition involves some combination of the integro-differential operators. This is possible, since the radiated and incoming fields do not depend on the type of the integro-differential operator [*Ergül and Gürel*, 2009]. Only the receiving patterns of the testing functions depend on the operator and the testing type, i.e., $\hat{\boldsymbol{t}} \cdot \boldsymbol{\mathcal{T}}$, $\hat{\boldsymbol{n}} \times \boldsymbol{\mathcal{T}}$, $\hat{\boldsymbol{t}} \cdot \boldsymbol{\mathcal{K}}$, and $\hat{\boldsymbol{n}} \times \boldsymbol{\mathcal{K}}$.

[21] 3. At the beginning of an aggregation stage, radiation patterns of the RWG functions are multiplied

with the coefficients provided by the iterative algorithm and combined to obtain the radiated fields of the clusters in the lowest level. In the aggregation stage performed for a region D_u, only the RWG functions located on the surface of the region (S_u) are considered. Besides, for the partitions $\overline{\boldsymbol{Z}}_u^{(12)}$ and $\overline{\boldsymbol{Z}}_u^{(22)}$, basis functions located on metallic surfaces are omitted.

[22] 4. At the end of a disaggregation stage, incoming fields are received by the testing functions. Similar to the aggregation stage, a disaggregation stage performed for a region D_u involves only the RWG functions located on the surface of the region. In addition, testing functions located on metallic surfaces do not receive incoming fields for the partitions $\overline{\boldsymbol{Z}}_u^{(21)}$ and $\overline{\boldsymbol{Z}}_u^{(22)}$.

[23] 5. The signs γ_m and γ_n in (9), (13), and (14), are introduced when the radiation patterns of the basis functions are combined or when the incoming fields are multiplied with the receiving patterns of the testing functions in the lowest level.

4. Block-Diagonal Preconditioning of JMCFIE

[24] MLFMA provides the solution of large problems by reducing the complexity of the matrix-vector multiplications required by the iterative solvers from $\mathcal{O}(N^2)$ to $\mathcal{O}(N \log N)$. For efficient solutions, however, the number of iterations should also be small, in addition to fast matrix-vector multiplications. In general, JMCFIE is a second-kind integral equation, and its Galerkin discretization involves well tested identity operators, which lead to well conditioned matrix equations [*Ylä-Oijala and Taskinen*, 2005a, 2005b; *Ylä-Oijala et al.*, 2005b]. Matrix equations obtained with JMCFIE are easy to solve iteratively, especially when the contrasts between the neighboring dielectric regions are low, i.e., permittivity and permeability do not change significantly across dielectric interfaces. However, iterative solutions of JMCFIE become difficult as the contrast increases [*Ylä-Oijala et al.*, 2005b; *Ylä-Oijala*, 2008; *Ergül and Gürel*, 2009], and effective preconditioners are required to reduce the number of iterations, especially when the problem size is large.

4.1. Effect of the Contrast in JMCFIE

[25] When a problem does not involve any metallic surface, the diagonal partitions of JMCFIE are identical. For composite structures with metallic surfaces, however, these partitions are not identical, and they have different sizes, which may deteriorate the numerical balance of the matrix equations. On the other hand, iterative solutions of JMCFIE become difficult with the increasing contrast, even in the case of nonmetallic objects. The main reason is the existence of off-diagonal partitions, which are numerically sensitive to the contrast. In general, off-diagonal partitions of JMCFIE are significantly unbalanced due to multiplications with η_u^{-1} and η_u in (13) and (14), respectively. Although this may not be critical for low contrasts, the off-diagonal partition $\overline{\boldsymbol{Z}}^{(21)}$ dominates the overall matrix, as the contrast of the object increases. As a result, the overall matrix equation becomes significantly unbalanced and difficult to solve iteratively.

[26] For a further analysis, we consider a special case involving a dielectric object in homogeneous space. Matrix elements in this case are derived explicitly in Appendix A. In general, the numerical significance of the off-diagonal $\overline{\boldsymbol{Z}}^{(21)}$ grows rapidly with the increasing contrast. Our investigations also show that a combined operator $(\eta_0 \boldsymbol{\mathcal{T}}_0 - \eta_1 \boldsymbol{\mathcal{T}}_1)$ presents a major contribution in $\overline{\boldsymbol{Z}}^{(21)}$ for relatively high contrasts. The related term can be written as

$$Z_{mn,\boldsymbol{\mathcal{T}}}^{(21)} = i\omega \int_{A_m} d\boldsymbol{r} \boldsymbol{t}_m(\boldsymbol{r}) \cdot \hat{\boldsymbol{n}}(\boldsymbol{r}) \times \left\{ \int_{A_n} d\boldsymbol{r}' \boldsymbol{b}_n(\boldsymbol{r}') [\mu_0 g_0(\boldsymbol{r}, \boldsymbol{r}') - \mu_1 g_1(\boldsymbol{r}, \boldsymbol{r}')] + \frac{1}{\omega^2} \int_{A_n} d\boldsymbol{r}' \nabla' \cdot \boldsymbol{b}_n(\boldsymbol{r}') \nabla \left[\frac{g_0(\boldsymbol{r}, \boldsymbol{r}')}{\epsilon_0} - \frac{g_1(\boldsymbol{r}, \boldsymbol{r}')}{\epsilon_1} \right] \right\}. \tag{20}$$

Using a Taylor series expansion for the exponential in the Green's function,

$$[\mu_0 g_0(\boldsymbol{r}, \boldsymbol{r}') - \mu_1 g_1(\boldsymbol{r}, \boldsymbol{r}')] = \frac{1}{4\pi R} \sum_{s=0}^{\infty} \frac{(i\omega R)^s}{s!} \left[\mu_0 (\mu_0 \epsilon_0)^{s/2} - \mu_1 (\mu_1 \epsilon_1)^{s/2} \right] \tag{21}$$

and

$$\nabla \left[\frac{g_0(\boldsymbol{r}, \boldsymbol{r}')}{\epsilon_0} - \frac{g_1(\boldsymbol{r}, \boldsymbol{r}')}{\epsilon_1} \right] = \frac{\hat{\boldsymbol{R}}}{4\pi R^2} \sum_{s=0}^{\infty} \frac{(i\omega R)^{s+1}}{s!} \left[\frac{(\mu_0 \epsilon_0)^{s/2+1/2}}{\epsilon_0} - \frac{(\mu_1 \epsilon_1)^{s/2+1/2}}{\epsilon_1} \right] - \frac{\hat{\boldsymbol{R}}}{4\pi R^2} \sum_{s=0}^{\infty} \frac{(i\omega R)^s}{s!} \left[\frac{(\mu_0 \epsilon_0)^{s/2}}{\epsilon_0} - \frac{(\mu_1 \epsilon_1)^{s/2}}{\epsilon_1} \right], \tag{22}$$

where $\boldsymbol{R} = (\boldsymbol{r} - \boldsymbol{r}') = \hat{\boldsymbol{R}} R$. We note that $1/R$ and $1/R^2$ singularities in (21) and (22) exist when $\mu_0 \neq \mu_1$ and $\epsilon_0 \neq \epsilon_1$, respectively. In addition, numerical values of the expressions in (21) and (22), thus the contribution of $(\eta_0 \boldsymbol{\mathcal{T}}_0 - \eta_1 \boldsymbol{\mathcal{T}}_1)$ in $\overline{\boldsymbol{Z}}^{(21)}$, grow rapidly with the increasing contrast. Finally, the resulting matrix equation becomes significantly unbalanced, due to large elements in $\overline{\boldsymbol{Z}}^{(21)}$.

4.2. Preconditioning

[27] In general, the matrix equation in (6) can be preconditioned as

$$(\overline{\boldsymbol{P}})^{-1} \cdot \begin{bmatrix} \overline{\boldsymbol{Z}}^{(11)} & \overline{\boldsymbol{Z}}^{(12)} \\ \overline{\boldsymbol{Z}}^{(21)} & \overline{\boldsymbol{Z}}^{(22)} \end{bmatrix} \cdot \begin{bmatrix} \boldsymbol{a}^J \\ \boldsymbol{a}^M \end{bmatrix} = (\overline{\boldsymbol{P}})^{-1} \cdot \begin{bmatrix} \boldsymbol{v}^{(1)} \\ \boldsymbol{v}^{(2)} \end{bmatrix}, \tag{23}$$

where $\overline{\boldsymbol{P}}$ is a $(N + N_D) \times (N + N_D)$ preconditioner matrix. In MLFMA, there are $\mathcal{O}(N)$ near-field interactions, which are calculated directly and are available for constructing preconditioners. These interactions are between the basis and testing functions that are located in the same cluster or in two touching clusters in the lowest level of the tree structure. During solutions with MLFMA, we reorder the RWG functions according to their positions in the multilevel tree. Let C be the number of clusters in the lowest level and $N(c)$ represent the number of RWG functions in cluster c = 1, 2,..., C. Then, the RWG functions in cluster c are indexed from $N^T(c)$ + 1 to $N^T(c)$ + $N(c)$, where

$$N^T(c) = \sum_{c'=1}^{c-1} N(c). \tag{24}$$

This way, the system matrix in (6) has a block structure, where each block represents the interaction of a pair of lowest-level clusters. In the sparse near-field matrix, only the blocks corresponding to the self interactions of the clusters or the interactions of two touching clusters involve nonzero elements.

[28] The block-diagonal preconditioner (BDP), which is based on using the self interactions of the lowest-level clusters, is commonly used to accelerate MLFMA solutions of electromagnetics problems involving perfectly conducting objects [*Song et al.*, 1997; *Chew et al.*, 2001]. The preconditioner matrix, which has a block-diagonal structure, can be inverted and used efficiently with $\mathcal{O}(N)$ complexity. Although BDP is successful in reducing the iteration counts for second-kind integral equations [*Song et al.*, 1997], such as the combined-field integral equation (CFIE), it may not accelerate the iterative solutions of first-kind integral equations [*Gürel and Ergül*, 2006], such as the electric field integral equation (EFIE). In fact, EFIE solutions are usually decelerated with BDP [*Gürel and Ergül*, 2003], and BDP is rarely useful for EFIE [*Ubeda et al.*, 2006; *Ergül et al.*, 2007].

4.3. Two-Partition Block-Diagonal Preconditioner

[29] A direct extension of BDP for dielectric problems, which we call 2PBDP, involves the self interactions of the lowest-level clusters in the diagonal partitions, i.e.,

$$\overline{\boldsymbol{P}}_{2P} \approx \begin{bmatrix} \overline{\boldsymbol{P}}^{(11)}_{N\times N} & 0 \\ 0 & \overline{\boldsymbol{P}}^{(22)}_{N_D\times N_D} \end{bmatrix}, \tag{25}$$

where

$$\overline{\boldsymbol{P}}^{(11)}_{N\times N} \approx \overline{\boldsymbol{Z}}^{(11)}_{N\times N} \tag{26}$$

$$\overline{\boldsymbol{P}}^{(22)}_{N_D\times N_D} \approx \overline{\boldsymbol{Z}}^{(22)}_{N_D\times N_D} \tag{27}$$

are block-diagonal matrices. Then, a preconditioned matrix equation can be written as

$$\begin{bmatrix} \overline{\boldsymbol{B}}^{(11)} \cdot \overline{\boldsymbol{Z}}^{(11)} & \overline{\boldsymbol{B}}^{(11)} \cdot \overline{\boldsymbol{Z}}^{(12)} \\ \overline{\boldsymbol{B}}^{(22)} \cdot \overline{\boldsymbol{Z}}^{(21)} & \overline{\boldsymbol{B}}^{(22)} \cdot \overline{\boldsymbol{Z}}^{(22)} \end{bmatrix} \cdot \begin{bmatrix} \boldsymbol{a}^J \\ \boldsymbol{a}^M \end{bmatrix} = \begin{bmatrix} \overline{\boldsymbol{B}}^{(11)} \cdot \boldsymbol{v}^{(1)} \\ \overline{\boldsymbol{B}}^{(22)} \cdot \boldsymbol{v}^{(2)} \end{bmatrix}, \tag{28}$$

where

$$\overline{\boldsymbol{B}}^{(11)}_{N\times N} = \left(\overline{\boldsymbol{P}}^{(11)}_{N\times N}\right)^{-1} \tag{29}$$

$$\overline{\boldsymbol{B}}^{(22)}_{N_D\times N_D} = \left(\overline{\boldsymbol{P}}^{(22)}_{N_D\times N_D}\right)^{-1} \tag{30}$$

are also block-diagonal matrices. As presented in section 5, 2PBDP accelerates iterative solutions of problems involving dielectric regions with relatively low contrasts. As the contrast increases, however, 2PBDP, which does not employ the large elements in $\overline{\boldsymbol{Z}}^{(21)}$, can be insufficient to accelerate the iterations. For those problems, better preconditioners are required to reduce the iteration counts and to increase the efficiency of the solutions.

4.4. Four-Partition Block-Diagonal Preconditioner

[30] To improve the iterative solutions of JMCFIE, we propose 4PBDP, which is based on using the diagonal blocks, i.e., self interactions of the lowest-level clusters, in all four partitions of the matrix equations. This way, some of the large elements in $\overline{\boldsymbol{Z}}^{(21)}$ are considered in constructing an effective preconditioner. The resulting preconditioner matrices are in the form of

$$\overline{\boldsymbol{P}}_{4P} \approx \begin{bmatrix} \overline{\boldsymbol{P}}^{(11)}_{N\times N} & \overline{\boldsymbol{P}}^{(12)}_{N\times N_D} \\ \overline{\boldsymbol{P}}^{(21)}_{N_D\times N} & \overline{\boldsymbol{P}}^{(22)}_{N_D\times N_D} \end{bmatrix}, \tag{31}$$

where $\overline{\boldsymbol{P}}^{(11)}_{N\times N}$ and $\overline{\boldsymbol{P}}^{(22)}_{N_D\times N_D}$ are block-diagonal matrices as in 2PBDP. The partitions

$$\overline{\boldsymbol{P}}^{(12)}_{N\times N_D} \approx \overline{\boldsymbol{Z}}^{(12)}_{N\times N_D} \tag{32}$$

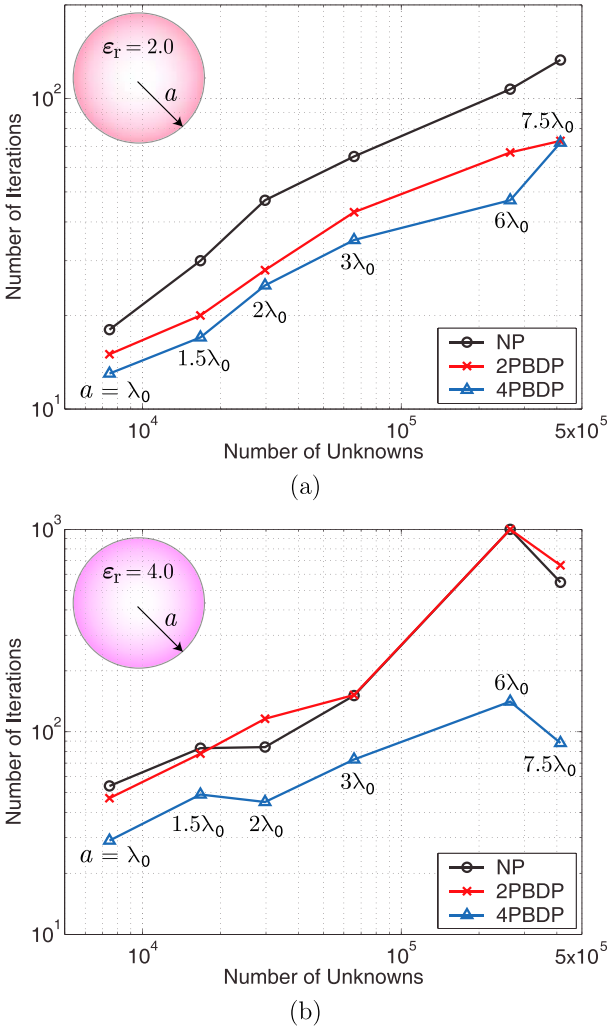

Figure 1. Iteration counts for the solution of scattering problems involving a dielectric sphere with a relative permittivity of (a) 2.0 and (b) 4.0, when the radius of the sphere is in the range of $0.75\lambda_0$ to $7.5\lambda_0$, where λ_0 is the wavelength in free space.

$$\overline{\boldsymbol{P}}^{(21)}_{N_D\times N} \approx \overline{\boldsymbol{Z}}^{(21)}_{N_D\times N} \tag{33}$$

are also block matrices involving the self interactions of the clusters. However, these partitions are square and block-diagonal only when a problem does not involve metallic surfaces ($N_D = N$); otherwise, they are rectangular matrices. In addition, the blocks in $\overline{\boldsymbol{P}}^{(12)}_{N\times N_D}$ and $\overline{\boldsymbol{P}}^{(21)}_{N_D\times N}$ are not necessarily square, and some of them can be rectangular, depending on the object and the clustering scheme in MLFMA.

[31] Using 4PBDP, a preconditioned matrix equation can be written as

$$\begin{bmatrix} \overline{\boldsymbol{B}}^{(11)} & \overline{\boldsymbol{B}}^{(12)} \\ \overline{\boldsymbol{B}}^{(21)} & \overline{\boldsymbol{B}}^{(22)} \end{bmatrix} \cdot \begin{bmatrix} \overline{\boldsymbol{Z}}^{(11)} & \overline{\boldsymbol{Z}}^{(12)} \\ \overline{\boldsymbol{Z}}^{(21)} & \overline{\boldsymbol{Z}}^{(22)} \end{bmatrix} \cdot \begin{bmatrix} \boldsymbol{a}^J \\ \boldsymbol{a}^M \end{bmatrix} = \begin{bmatrix} \overline{\boldsymbol{B}}^{(11)} \cdot \boldsymbol{v}^{(1)} + \overline{\boldsymbol{B}}^{(12)} \cdot \boldsymbol{v}^{(2)} \\ \overline{\boldsymbol{B}}^{(21)} \cdot \boldsymbol{v}^{(1)} + \overline{\boldsymbol{B}}^{(22)} \cdot \boldsymbol{v}^{(2)} \end{bmatrix}, \tag{34}$$

where

$$\overline{\boldsymbol{B}}^{(11)}_{N\times N} = \left(\overline{\boldsymbol{P}}^{(11)}_{N\times N}\right)^{-1} + \left(\overline{\boldsymbol{P}}^{(11)}_{N\times N}\right)^{-1} \cdot \overline{\boldsymbol{P}}^{(12)}_{N\times N_D} \cdot \left(\overline{\boldsymbol{S}}_{N_D\times N_D}\right)^{-1} \cdot \overline{\boldsymbol{P}}^{(21)}_{N_D\times N} \cdot \left(\overline{\boldsymbol{P}}^{(11)}_{N\times N}\right)^{-1} \tag{35}$$

$$\overline{\boldsymbol{B}}^{(12)}_{N\times N_D} = -\left(\overline{\boldsymbol{P}}^{(11)}_{N\times N}\right)^{-1} \cdot \overline{\boldsymbol{P}}^{(12)}_{N\times N_D} \cdot \left(\overline{\boldsymbol{S}}_{N_D\times N_D}\right)^{-1} \tag{36}$$

$$\overline{\boldsymbol{B}}^{(21)}_{N_D\times N} = -\left(\overline{\boldsymbol{S}}_{N_D\times N_D}\right)^{-1} \cdot \overline{\boldsymbol{P}}^{(21)}_{N_D\times N} \cdot \left(\overline{\boldsymbol{P}}^{(11)}_{N\times N}\right)^{-1} \tag{37}$$

$$\overline{\boldsymbol{B}}^{(22)}_{N_D\times N_D} = \left(\overline{\boldsymbol{S}}_{N_D\times N_D}\right)^{-1} \tag{38}$$

and

$$\overline{\boldsymbol{S}}_{N_D\times N_D} = \overline{\boldsymbol{P}}^{(22)}_{N_D\times N_D} - \overline{\boldsymbol{P}}^{(21)}_{N_D\times N} \cdot \left(\overline{\boldsymbol{P}}^{(11)}_{N\times N}\right)^{-1} \cdot \overline{\boldsymbol{P}}^{(12)}_{N\times N_D} \tag{39}$$

is the Schur complement of $\overline{\boldsymbol{P}}^{(11)}_{N\times N}$ [*Gürel and Chew*, 1990]. Matrix operations in (35)–(39), i.e., matrix-matrix multiplications, the inversion of $\overline{\boldsymbol{P}}^{(11)}_{N\times N}$, and the inversion of $\overline{\boldsymbol{S}}_{N_D\times N_D}$ can be performed efficiently in $\mathcal{O}(N)$ time using $\mathcal{O}(N)$ memory. Our numerical experiments show that the extra cost of 4PBDP with respect to 2PBDP is always negligible, considering the overall cost of the solutions with MLFMA. Nevertheless, as demonstrated in the next section, 4PBDP can significantly improve the efficiency of solutions by reducing iteration counts, and it is especially useful when the acceleration provided by 2PBDP is not sufficient.

5. Results

[32] In this section, we present iterative solutions for various scattering problems and investigate their iteration counts when the solutions are accelerated with 2PBDP and 4PBDP, in addition to the no-preconditioner (NP) case. Scatterers are illuminated by a plane wave propagating in the $-x$ direction with the electric field polarized in the y direction. Surfaces are discretized with about $\lambda_0/10$ mesh size, where λ_0 is the wavelength in medium D_0 (free space) that extends to infinity. Iterative solutions are performed using the biconjugate-gradient-stabilized

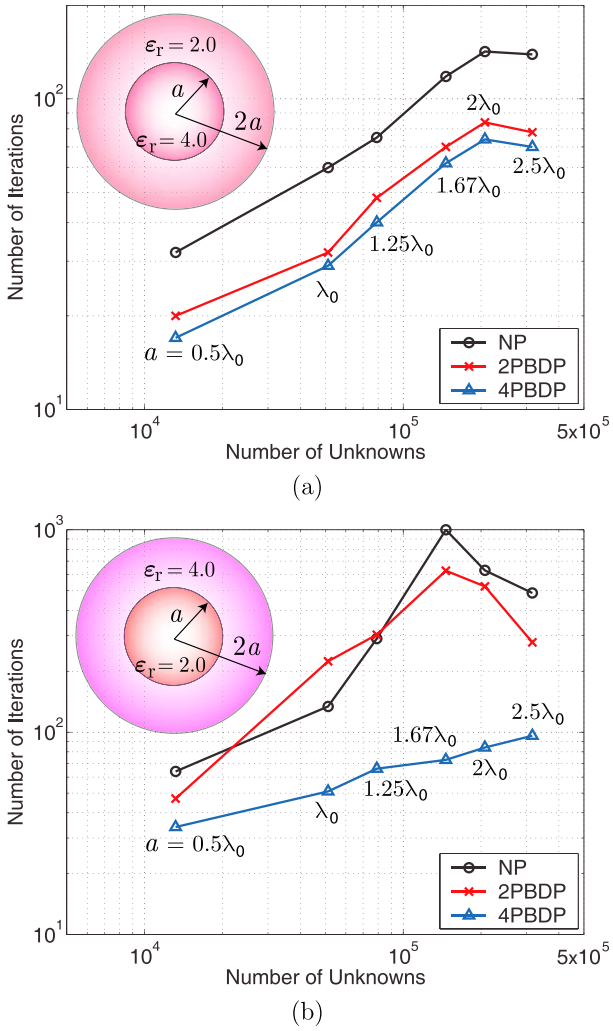

Figure 2. Iteration counts for the solution of scattering problems involving a dielectric sphere of radius a coated with a dielectric shell of radius $2a$, where a changes from $0.5\lambda_0$ to $2.5\lambda_0$. (a) Low-contrast case when the relative permittivities of the core and shell are 4.0 and 2.0, respectively. (b) High-contrast case when the relative permittivities of the core and shell are 2.0 and 4.0, respectively.

(BiCGStab) algorithm [*Van der Vorst*, 1992], which is known to provide rapid solutions for second-kind integral equations. In all solutions, matrix-vector multiplications are accelerated via MLFMA, and the relative residual error for the iterative convergence is set to 10^{-3}.

[33] First, we consider scattering problems involving a dielectric sphere. Figure 1a presents the number of BiCGStab iterations when the relative permittivity of the sphere is 2.0 and the radius of the sphere (a) changes from λ_0 to $7.5\lambda_0$. Discretizations of problems lead to 4142 and 412,998 unknowns, respectively, for radii $0.75\lambda_0$ and $7.5\lambda_0$. As depicted in Figure 1a, 2PBDP accelerates the iterative convergence substantially, compared to the NP case. Using 4PBDP further reduces the iteration counts, but the improvement with respect to 4PBDP is considerable only when $a = 6\lambda_0$. Figure 1b presents the iteration counts with respect to the number of unknowns when the relative permittivity of the sphere is 4.0. In general, iterative solutions become difficult with increasing contrast. For a radius of $6\lambda_0$, convergence is not achieved in 1000 iterations without preconditioning. Furthermore, unlike the low-contrast ($\epsilon_r = 2.0$) case, 2PBDP is unable to reduce the iteration counts when $\epsilon_r = 4.0$. When we use 4PBDP, however, iterative solutions are accelerated significantly, and we obtain efficient solutions.

[34] Figure 2 depicts iteration counts for the solution of scattering problems involving a spherical object with multiple dielectric regions. A dielectric sphere of radius a is coated with a dielectric shell of radius $2a$, where a changes from $0.5\lambda_0$ to $2.5\lambda_0$. Discretizations of problems lead to 13,176 and 316,032 unknowns, respectively, when $a = 0.5\lambda_0$ and $a = 2.5\lambda_0$. Figure 2a presents iteration counts with respect to the number of unknowns when the relative permittivities of the core and the shell are 4.0 and 2.0, respectively. In this case, 2PBDP reduces iteration counts substantially in comparison to the NP case, while 4PBDP does not provide a significant improvement over 2PBDP. On the other hand, when the permittivity of the shell and the core are exchanged, we obtain the iteration counts depicted in Figure 2b, where 4PBDP presents a superior performance in comparison to 2PBDP. Owing to the relatively high contrast between the shell and free space, solutions of JMCFIE become difficult without preconditioning. For example, when $a = 1.67\lambda_0$, convergence cannot be achieved in 1000 iterations. 2PBDP accelerates the convergence for large problems, but the improvement is not sufficient. Using 4PBDP, the number of iterations is less than 100 for all solutions in Figure 2.

[35] Next, we consider iterative solutions of scattering problems involving a spherical composite object. In this case, a metallic sphere of radius a is coated with a dielectric shell of radius $2a$, where a changes from $0.5\lambda_0$ to $2.5\lambda_0$. Figure 3 presents iteration counts with respect to the number of iterations. Similar to the previous example, 2PBDP reduces the iteration counts significantly for the low-contrast case, i.e., when the relative permittivity of the shell is 2.0, as depicted in Figure 3a. In this case, 4PBDP provides some improvement over 2PBDP, as the problem size grows. When the relative permittivity of the shell is 4.0, however, 4PBDP accelerates the iterative solutions significantly, compared to 2PBDP. In fact, 2PBDP decelerates the solutions for large problems, and there is a large discrepancy between

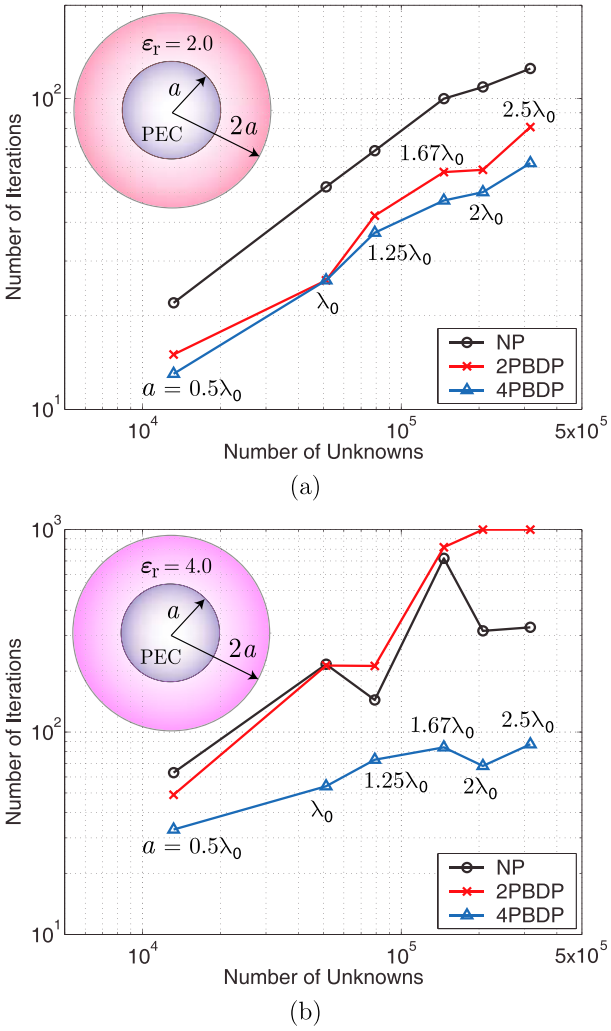

Figure 3. Iteration counts for the solution of scattering problems involving a perfectly conducting sphere of radius a coated with a dielectric shell of radius $2a$, where a changes from $0.5\lambda_0$ to $2.5\lambda_0$. The relative permittivity of the shell is (a) 2.0 and (b) 4.0.

the performances of 2PBDP and 4PBDP. Using 4PBDP, the number of iterations is again less than 100 for all solutions in Figure 3.

[36] We also consider electromagnetics problems involving dielectric and composite objects with sharp edges and corners. Figure 4 presents iteration counts for the solution of scattering problems involving a coated dielectric cube. The core and shell have edges of a and $2a$, respectively, where a changes from $0.5\lambda_0$ to $2.5\lambda_0$. Faces of the object are parallel to the coordinate axes. Discretizations of problems lead to matrix equations with 9864 to 228,132 unknowns. Figure 4a depicts iteration counts as a function of the number of unknowns, when the relative permittivities of the core and shell are 4.0 and 2.0, respectively. The results are similar to those for the spherical object depicted in Figure 2a, i.e., 2PBDP accelerates the iterative solutions significantly, and 4PBDP further reduces the iteration counts slightly compared to 2PBDP. When the relative permittivities of the core and shell are exchanged, however, 4PBDP performs much better than 2PBDP, as depicted in Figure 4b. On the other hand, unlike the solutions of the

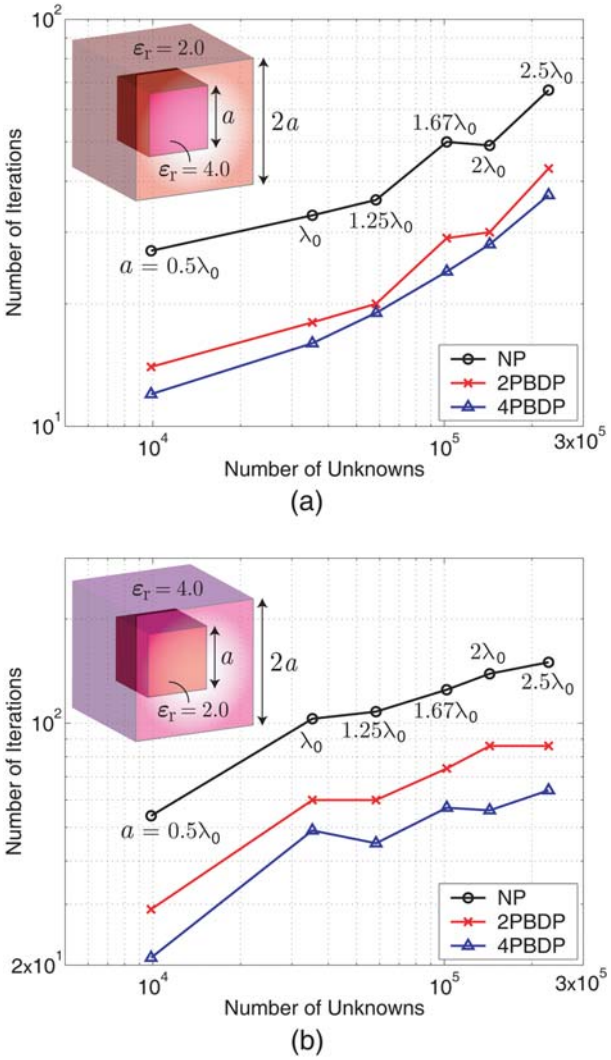

Figure 4. Iteration counts for the solution of scattering problems involving a dielectric cube coated with a dielectric shell. The core and shell have edges of a and $2a$, respectively, where a changes from $0.5\lambda_0$ to $2.5\lambda_0$. (a) Low-contrast case when the relative permittivities of the core and shell are 4.0 and 2.0, respectively. (b) High-contrast case when the relative permittivities of the core and shell are 2.0 and 4.0, respectively.

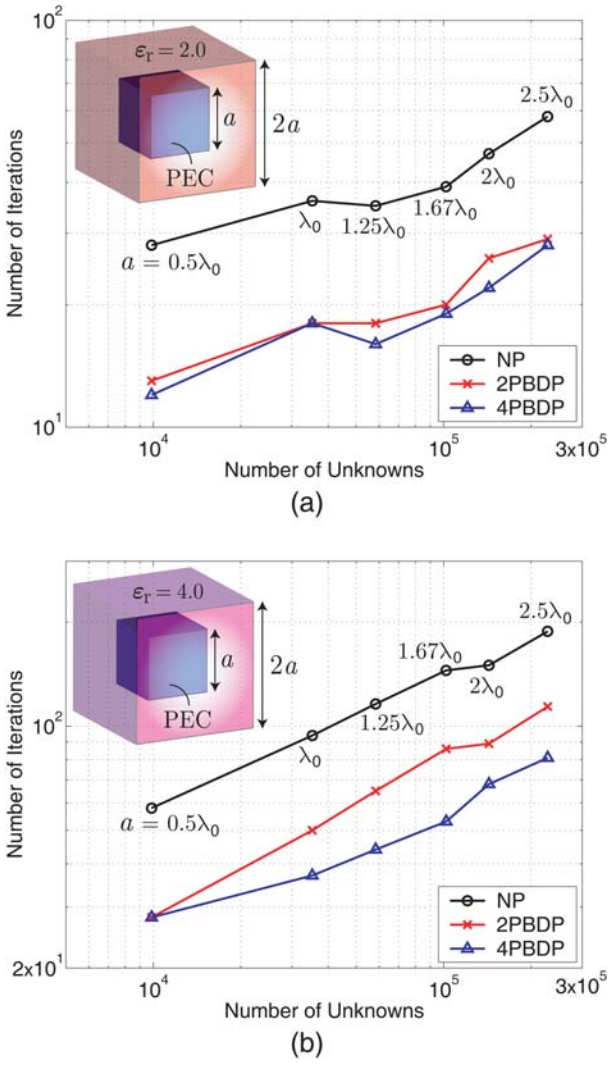

Figure 5. Iteration counts for the solution of scattering problems involving a perfectly conducting cube coated with a dielectric shell. The core and shell have edges of a and $2a$, respectively, where a changes from $0.5\lambda_0$ to $2.5\lambda_0$. The relative permittivity of the shell is (a) 2.0 and (b) 4.0.

spherical object in Figure 2b, 2PBDP is also effective for the high-contrast case in Figure 4b. This is probably due to the larger numbers of elements being used in constructing 2PBDP for the cubic object, i.e., the lowest-level clusters in the multilevel tree are more populated for the cubic object than for the spherical object. Nevertheless, 4PBDP is again preferable for all solutions in Figure 4.

[37] Figure 5 presents the solution of scattering problems involving a coated metallic cube. The sizes of the core and shell are the same as those in the coated dielectric cube. Similar to previous examples, 4PBDP provides the most efficient results, and it presents improved convergence in comparison to 2PBDP, when the contrast is relatively high.

[38] In Figure 6, we present the solution of scattering problems involving a spherical object with three dielectric regions. A dielectric sphere of radius $0.3a$ is coated with two dielectric shells of radii $0.5a$ and a, where a changes from $2\lambda_0$ to $2.6\lambda_0$. Relative permittivities of the core, inner shell, and outer shell are 1.44, 1.96, and 4.0, respectively. Only one discretization involving 215,304 unknowns is used for the entire frequency range. As depicted in Figure 6, solutions are performed efficiently with maximum 101 iterations using 4PBDP. Figure 6 also presents the normalized radar cross section (RCS/πa^2) in the backscattering direction as a function of a in terms of the wavelength. We observe that computational values are in agreement with analytical values obtained by Mie-series solutions.

[39] Finally, to demonstrate the effectiveness of an implementation involving MLFMA, JMCFIE, and 4PBDP,

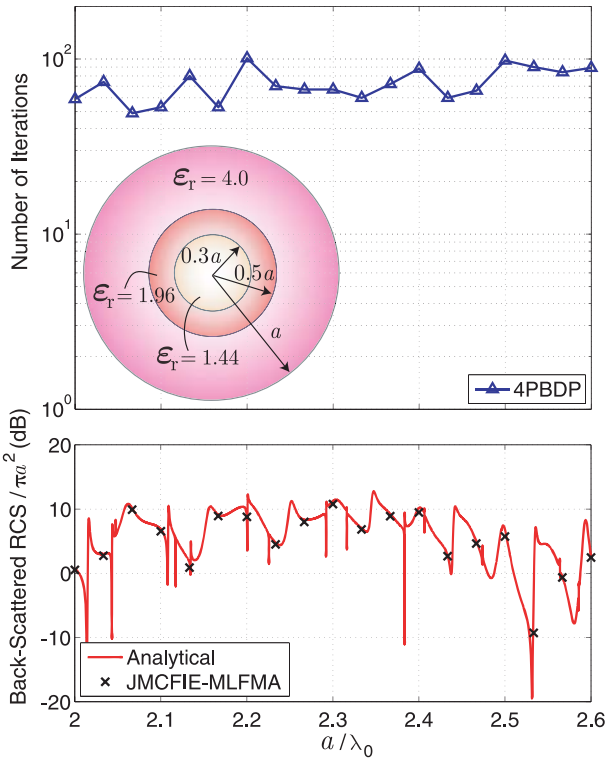

Figure 6. Iteration counts for the solution of scattering problems involving a dielectric sphere of radius $0.3a$ coated with two dielectric shells of radii $0.5a$ and a, where a changes from $2\lambda_0$ to $2.6\lambda_0$. Relative permittivities of the core, inner shell, and outer shell are 1.44, 1.96, and 4.0, respectively. Normalized RCS (RCS/πa^2) of the structure in the backscattering direction is also plotted as a function of a in terms of wavelength.

we present the solution of large scattering problems discretized with 1,264,128 unknowns. A sphere of radius $5\lambda_0$ is placed inside another sphere of radius $10\lambda_0$. We consider four different cases: (1) Relative permittivities of the core and shell are 4.0 and 2.0, respectively. (2) Relative permittivities of the core and shell are 2.0 and 4.0, respectively. (3) The core is metallic and the relative permittivity of the shell is 2.0. (4) The core is metallic and the relative permittivity of the shell is 4.0.

[40] Scattering problems are solved via 6-level MLFMA, and the iteration counts are 101, 283, 75, and 187, respectively, for 10^{-3} residual error. Figures 7 and 8 present the normalized bistatic RCS (RCS/λ_0^2) values on the *x*-*z* plane, where 0° and 180° correspond to the forward scattering and backscattering directions, respectively. We observe that computational and analytical results agree perfectly.

6. Concluding Remarks

[41] In this paper, we present an efficient solution of JMCFIE using MLFMA and block-diagonal preconditioners. We provide the details of an MLFMA implementation for the solution of electromagnetics problems involving multiple dielectric and metallic regions. In general, JMCFIE is a preferable formulation that provides well conditioned matrix equations that are easy to solve iteratively. However, iterative solutions of JMCFIE can be difficult for problems involving dielectric regions with relatively high contrasts. This is mostly due to the numerical imbalance of the off-diagonal partitions of the matrix equations obtained with JMCFIE. To accelerate the iterative solutions, we present 4PBDP, which is an efficient preconditioner based on using the diagonal blocks in all four partitions of the matrix equations. We show that 4PBDP reduces the iteration counts significantly and performs better than the standard 2PBDP, which can be insufficient to improve the iterative convergence as the contrast increases.

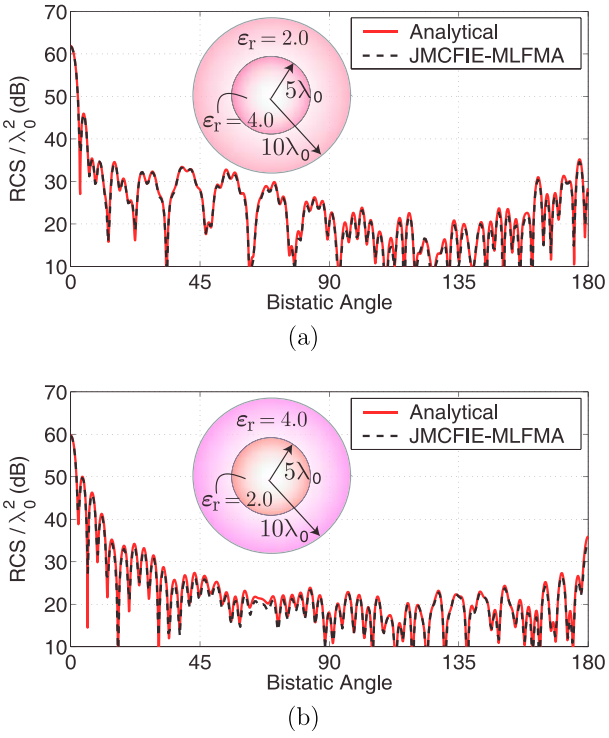

Figure 7. Normalized bistatic RCS (RCS/λ_0^2) of a structure involving spheres of radii $5\lambda_0$ and $10\lambda_0$, when (a) relative permittivities of the core and shell are 4.0 and 2.0, respectively, and (b) relative permittivities of the core and shell are 2.0 and 4.0, respectively.

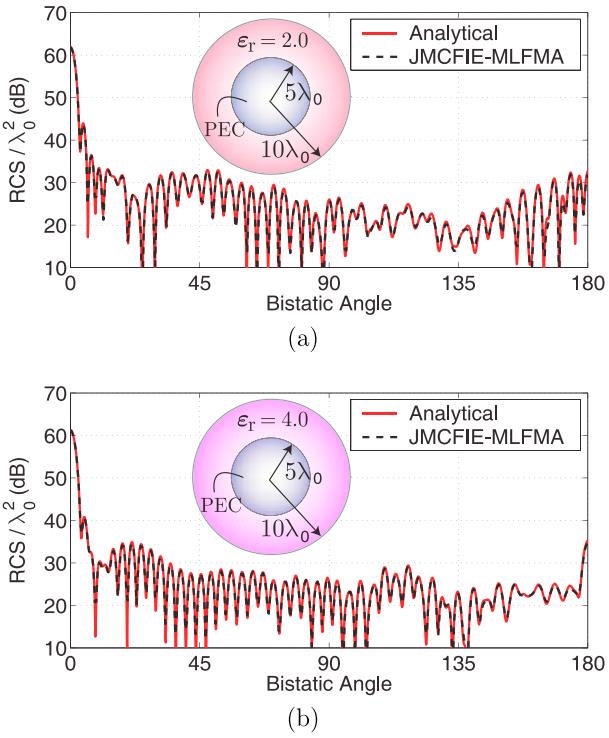

Figure 8. Normalized bistatic RCS (RCS/λ_0^2) of a structure involving spheres of radii $5\lambda_0$ and $10\lambda_0$, when (a) the core is metallic and the relative permittivity of the shell is 2.0, and (b) the core is metallic and the relative permittivity of the shell is 4.0.

Appendix A

[42] In this Appendix A, we present the matrix equations for the special cases depicted in Figure A1, i.e., a

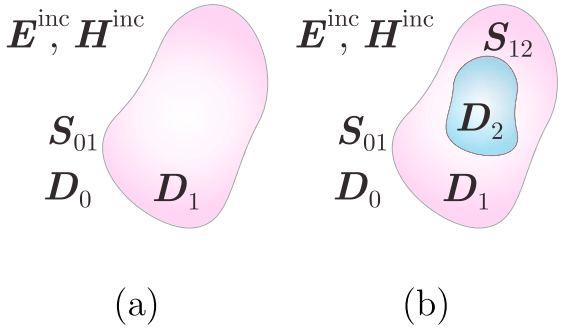

Figure A1. Electromagnetics problems involving (a) a single dielectric object and (b) a coated dielectric or metallic object located in homogeneous space.

dielectric object and a coated dielectric or metallic object in homogeneous space. We assume that the incident fields exist only in region D_0, which extends to infinity.

[43] In the case of a dielectric object as depicted in Figure A1a, there are two regions, namely, D_0 and D_1. Since there is no metallic surface, $N_D = N$, and the size of the matrix equation obtained from the discretization of JMCFIE is $2N \times 2N$. All RWG functions are located on the same surface, and each matrix element involves two sets of contributions due to the interactions of the basis and testing functions through the regions D_0 and D_1. Using (9), (13), and (14), we obtain

$$Z_{mn}^{(11)} = Z_{mn}^{(22)} = -\int_{A_m} d\boldsymbol{r}\boldsymbol{t}_m(\boldsymbol{r}) \cdot \boldsymbol{b}_n(\boldsymbol{r}) + \int_{A_m} d\boldsymbol{r}\boldsymbol{t}_m(\boldsymbol{r}) \cdot \hat{\boldsymbol{n}}(\boldsymbol{r}) \times [\boldsymbol{\mathcal{K}}_0 - \boldsymbol{\mathcal{K}}_1]\{\boldsymbol{b}_n\}(\boldsymbol{r}) + \int_{A_m} d\boldsymbol{r}\boldsymbol{t}_m(\boldsymbol{r}) \cdot [\boldsymbol{\mathcal{T}}_0 + \boldsymbol{\mathcal{T}}_1]\{\boldsymbol{b}_n\}(\boldsymbol{r}), \tag{A1}$$

$$Z_{mn}^{(12)} = \frac{1}{2}\left(\eta_1^{-1} - \eta_0^{-1}\right) \int_{A_m} d\boldsymbol{r}\boldsymbol{t}_m(\boldsymbol{r}) \cdot \hat{\boldsymbol{n}}(\boldsymbol{r}) \times \boldsymbol{b}_n(\boldsymbol{r}) + \int_{A_m} d\boldsymbol{r}\boldsymbol{t}_m(\boldsymbol{r}) \cdot \hat{\boldsymbol{n}}(\boldsymbol{r}) \times \left[\eta_0^{-1}\boldsymbol{\mathcal{T}}_0 - \eta_1^{-1}\boldsymbol{\mathcal{T}}_1\right]\{\boldsymbol{b}_n\}(\boldsymbol{r}) - \int_{A_m} d\boldsymbol{r}\boldsymbol{t}_m(\boldsymbol{r}) \cdot \left[\eta_0^{-1}\boldsymbol{\mathcal{K}}_0 + \eta_1^{-1}\boldsymbol{\mathcal{K}}_1\right]\{\boldsymbol{b}_n\}(\boldsymbol{r}), \tag{A2}$$

$$Z_{mn}^{(21)} = \frac{1}{2}(\eta_0 - \eta_1) \int_{A_m} d\boldsymbol{r}\boldsymbol{t}_m(\boldsymbol{r}) \cdot \hat{\boldsymbol{n}}(\boldsymbol{r}) \times \boldsymbol{b}_n(\boldsymbol{r}) - \int_{A_m} d\boldsymbol{r}\boldsymbol{t}_m(\boldsymbol{r}) \cdot \hat{\boldsymbol{n}}(\boldsymbol{r}) \times [\eta_0\boldsymbol{\mathcal{T}}_0 - \eta_1\boldsymbol{\mathcal{T}}_1]\{\boldsymbol{b}_n\}(\boldsymbol{r}) + \int_{A_m} d\boldsymbol{r}\boldsymbol{t}_m(\boldsymbol{r}) \cdot [\eta_0\boldsymbol{\mathcal{K}}_0 + \eta_1\boldsymbol{\mathcal{K}}_1]\{\boldsymbol{b}_n\}(\boldsymbol{r}) \tag{A3}$$

for $m, n = 1, 2, \ldots, N$. In addition, by testing the incident electric and magnetic fields, elements of the RHS vector can be calculated as

$$v_m^{(1)} = -\int_{A_m} d\boldsymbol{r}\boldsymbol{t}_m(\boldsymbol{r}) \cdot \hat{\boldsymbol{n}}(\boldsymbol{r}) \times \boldsymbol{H}_0^{inc}(\boldsymbol{r}) - \eta_0^{-1} \int_{A_m} d\boldsymbol{r}\boldsymbol{t}_m(\boldsymbol{r}) \cdot \boldsymbol{E}_0^{inc}(\boldsymbol{r}), \tag{A4}$$

$$v_m^{(2)} = \int_{A_m} d\boldsymbol{r}\boldsymbol{t}_m(\boldsymbol{r}) \cdot \hat{\boldsymbol{n}}(\boldsymbol{r}) \times \boldsymbol{E}_0^{inc}(\boldsymbol{r}) - \eta_0 \int_{A_m} d\boldsymbol{r}\boldsymbol{t}_m(\boldsymbol{r}) \cdot \boldsymbol{H}_0^{inc}(\boldsymbol{r}) \tag{A5}$$

for $m = 1, 2, \ldots, N$.

[44] In the case of a coated dielectric object, there are three nonmetallic regions, namely, D_0, D_1, and D_2, while D_1 is between D_0 and D_2. Since there is no metallic surface, $N_D = N$, and the size of the resulting matrix equation is again $2N \times 2N$. Let the first N_{01} RWG functions and the remaining $N_{12} = (N - N_{01})$ RWG functions be defined on surfaces S_{01} and S_{12}, respectively. Each partition in (6) can be divided into four subpartitions, i.e.,

$$\overline{\boldsymbol{Z}}^{(ab)} = \begin{bmatrix} \overline{\boldsymbol{Z}}^{(ab,11)} & \overline{\boldsymbol{Z}}^{(ab,12)} \\ \overline{\boldsymbol{Z}}^{(ab,21)} & \overline{\boldsymbol{Z}}^{(ab,22)} \end{bmatrix}_{N \times N} \tag{A6}$$

for $a = 1, 2$ and $b = 1, 2$. In (A6), $\overline{\boldsymbol{Z}}^{(ab,11)}$ and $\overline{\boldsymbol{Z}}^{(ab,22)}$ represent $N_{01} \times N_{01}$ and $N_{12} \times N_{12}$ matrices containing the interactions of the RWG functions located on S_{01} and S_{12}, respectively. Calculations of these interactions are similar to those in (A1)–(A3). For $m, n = 1, 2, \ldots, N_{01}$,

$$Z_{mn}^{(11,11)} = Z_{mn}^{(22,11)} = -\int_{A_m} d\boldsymbol{r}\boldsymbol{t}_m(\boldsymbol{r}) \cdot \boldsymbol{b}_n(\boldsymbol{r}) + \int_{A_m} d\boldsymbol{r}\boldsymbol{t}_m(\boldsymbol{r}) \cdot \hat{\boldsymbol{n}}(\boldsymbol{r}) \times [\boldsymbol{\mathcal{K}}_0 - \boldsymbol{\mathcal{K}}_1]\{\boldsymbol{b}_n\}(\boldsymbol{r}) + \int_{A_m} d\boldsymbol{r}\boldsymbol{t}_m(\boldsymbol{r}) \cdot [\boldsymbol{\mathcal{T}}_0 + \boldsymbol{\mathcal{T}}_1]\{\boldsymbol{b}_n\}(\boldsymbol{r}), \tag{A7}$$

$$Z_{mn}^{(12,11)} = \frac{1}{2}\left(\eta_1^{-1} - \eta_0^{-1}\right) \int_{A_m} d\boldsymbol{r}\boldsymbol{t}_m(\boldsymbol{r}) \cdot \hat{\boldsymbol{n}}(\boldsymbol{r}) \times \boldsymbol{b}_n(\boldsymbol{r}) + \int_{A_m} d\boldsymbol{r}\boldsymbol{t}_m(\boldsymbol{r}) \cdot \hat{\boldsymbol{n}}(\boldsymbol{r}) \times \left[\eta_0^{-1}\boldsymbol{\mathcal{T}}_0 - \eta_1^{-1}\boldsymbol{\mathcal{T}}_1\right]\{\boldsymbol{b}_n\}(\boldsymbol{r}) - \int_{A_m} d\boldsymbol{r}\boldsymbol{t}_m(\boldsymbol{r}) \cdot \left[\eta_0^{-1}\boldsymbol{\mathcal{K}}_0 + \eta_1^{-1}\boldsymbol{\mathcal{K}}_1\right]\{\boldsymbol{b}_n\}(\boldsymbol{r}), \tag{A8}$$

$$Z_{mn}^{(21,11)} = \frac{1}{2}(\eta_0 - \eta_1)\int_{A_m} d\boldsymbol{r}\boldsymbol{t}_m(\boldsymbol{r})\cdot\hat{\boldsymbol{n}}(\boldsymbol{r})\times\boldsymbol{b}_n(\boldsymbol{r}) - \int_{A_m} d\boldsymbol{r}\boldsymbol{t}_m(\boldsymbol{r})\cdot\hat{\boldsymbol{n}}(\boldsymbol{r})\times[\eta_0\boldsymbol{\mathcal{T}}_0 - \eta_1\boldsymbol{\mathcal{T}}_1]\{\boldsymbol{b}_n\}(\boldsymbol{r}) + \int_{A_m} d\boldsymbol{r}\boldsymbol{t}_m(\boldsymbol{r})\cdot[\eta_0\boldsymbol{\mathcal{K}}_0 + \eta_1\boldsymbol{\mathcal{K}}_1]\{\boldsymbol{b}_n\}(\boldsymbol{r}). \quad \text{(A9)}$$

For m, n = (N_{01} + 1), (N_{01} + 2),. . ., (N_{01} + N_{12}), and (m', n') = ($m - N_{01}$, $n - N_{01}$),

$$Z_{m'n'}^{(11,22)} = Z_{m'n'}^{(22,22)} = -\int_{A_m} d\boldsymbol{r}\boldsymbol{t}_m(\boldsymbol{r})\cdot\boldsymbol{b}_n(\boldsymbol{r}) + \int_{A_m} d\boldsymbol{r}\boldsymbol{t}_m(\boldsymbol{r})\cdot\hat{\boldsymbol{n}}(\boldsymbol{r})\times[\boldsymbol{\mathcal{K}}_1 - \boldsymbol{\mathcal{K}}_2]\{\boldsymbol{b}_n\}(\boldsymbol{r}) + \int_{A_m} d\boldsymbol{r}\boldsymbol{t}_m(\boldsymbol{r})\cdot[\boldsymbol{\mathcal{T}}_1 + \boldsymbol{\mathcal{T}}_2]\{\boldsymbol{b}_n\}(\boldsymbol{r}), \quad \text{(A10)}$$

$$Z_{m'n'}^{(12,22)} = \frac{1}{2}\left(\eta_2^{-1} - \eta_1^{-1}\right)\int_{A_m} d\boldsymbol{r}\boldsymbol{t}_m(\boldsymbol{r})\cdot\hat{\boldsymbol{n}}(\boldsymbol{r})\times\boldsymbol{b}_n(\boldsymbol{r}) + \int_{A_m} d\boldsymbol{r}\boldsymbol{t}_m(\boldsymbol{r})\cdot\hat{\boldsymbol{n}}(\boldsymbol{r}) \times \left[\eta_1^{-1}\boldsymbol{\mathcal{T}}_1 - \eta_2^{-1}\boldsymbol{\mathcal{T}}_2\right]\{\boldsymbol{b}_n\}(\boldsymbol{r}) - \int_{A_m} d\boldsymbol{r}\boldsymbol{t}_m(\boldsymbol{r})\cdot\left[\eta_1^{-1}\boldsymbol{\mathcal{K}}_1 + \eta_2^{-1}\boldsymbol{\mathcal{K}}_2\right]\{\boldsymbol{b}_n\}(\boldsymbol{r}), \quad \text{(A11)}$$

$$Z_{m'n'}^{(21,22)} = \frac{1}{2}(\eta_1 - \eta_2)\int_{A_m} d\boldsymbol{r}\boldsymbol{t}_m(\boldsymbol{r})\cdot\hat{\boldsymbol{n}}(\boldsymbol{r})\times\boldsymbol{b}_n(\boldsymbol{r}) - \int_{A_m} d\boldsymbol{r}\boldsymbol{t}_m(\boldsymbol{r})\cdot\hat{\boldsymbol{n}}(\boldsymbol{r}) \times [\eta_1\boldsymbol{\mathcal{T}}_1 - \eta_2\boldsymbol{\mathcal{T}}_2]\{\boldsymbol{b}_n\}(\boldsymbol{r}) + \int_{A_m} d\boldsymbol{r}\boldsymbol{t}_m(\boldsymbol{r})\cdot[\eta_1\boldsymbol{\mathcal{K}}_1 + \eta_2\boldsymbol{\mathcal{K}}_2]\{\boldsymbol{b}_n\}(\boldsymbol{r}). \quad \text{(A12)}$$

On the other hand, the off-diagonal subpartitions, i.e., $\overline{\boldsymbol{Z}}^{(ab,12)}$ and $\overline{\boldsymbol{Z}}^{(ab,21)}$, involve the interactions of the basis and testing functions that are located on different surfaces. These basis and testing functions interact only through the region D_1. For $m = 1, 2,\ldots, N_{01}$, $n = (N_{01} + 1)$, (N_{01} + 2),. . ., (N_{01} + N_{12}), and $n' = n - N_{01}$,

$$Z_{mn'}^{(11,12)} = Z_{mn'}^{(22,12)} = \frac{1}{2}\int_{A_m} d\boldsymbol{r}\boldsymbol{t}_m(\boldsymbol{r})\cdot\boldsymbol{b}_n(\boldsymbol{r}) + \int_{A_m} d\boldsymbol{r}\boldsymbol{t}_m(\boldsymbol{r})\cdot\hat{\boldsymbol{n}}(\boldsymbol{r})\times\boldsymbol{\mathcal{K}}_1\{\boldsymbol{b}_n\}(\boldsymbol{r}) - \int_{A_m} d\boldsymbol{r}\boldsymbol{t}_m(\boldsymbol{r})\cdot\boldsymbol{\mathcal{T}}_1\{\boldsymbol{b}_n\}(\boldsymbol{r}), \quad \text{(A13)}$$

$$Z_{mn'}^{(12,12)} = -\frac{\eta_1^{-1}}{2}\int_{A_m} d\boldsymbol{r}\boldsymbol{t}_m(\boldsymbol{r})\cdot\hat{\boldsymbol{n}}(\boldsymbol{r})\times\boldsymbol{b}_n(\boldsymbol{r}) + \eta_1^{-1}\int_{A_m} d\boldsymbol{r}\boldsymbol{t}_m(\boldsymbol{r})\cdot\hat{\boldsymbol{n}}(\boldsymbol{r})\times\boldsymbol{\mathcal{T}}_1\{\boldsymbol{b}_n\}(\boldsymbol{r}) + \eta_1^{-1}\int_{A_m} d\boldsymbol{r}\boldsymbol{t}_m(\boldsymbol{r})\cdot\boldsymbol{\mathcal{K}}_1\{\boldsymbol{b}_n\}(\boldsymbol{r}), \quad \text{(A14)}$$

$$Z_{mn'}^{(21,12)} = \frac{\eta_1}{2}\int_{A_m} d\boldsymbol{r}\boldsymbol{t}_m(\boldsymbol{r})\cdot\hat{\boldsymbol{n}}(\boldsymbol{r})\times\boldsymbol{b}_n(\boldsymbol{r}) - \eta_1\int_{A_m} d\boldsymbol{r}\boldsymbol{t}_m(\boldsymbol{r})\cdot\hat{\boldsymbol{n}}(\boldsymbol{r})\times\boldsymbol{\mathcal{T}}_1\{\boldsymbol{b}_n\}(\boldsymbol{r}) - \eta_1\int_{A_m} d\boldsymbol{r}\boldsymbol{t}_m(\boldsymbol{r})\cdot\boldsymbol{\mathcal{K}}_1\{\boldsymbol{b}_n\}(\boldsymbol{r}). \quad \text{(A15)}$$

For $m = (N_{01}+1), (N_{01}+2),\ldots,(N_{01}+N_{12})$, $n = 1, 2,\ldots, N_{01}$, N_{01}, and $m' = m - N_{01}$,

$$Z_{m'n}^{(11,21)} = Z_{m'n}^{(22,21)} = \frac{1}{2}\int_{A_m} d\boldsymbol{r}\boldsymbol{t}_m(\boldsymbol{r})\cdot\boldsymbol{b}_n(\boldsymbol{r}) - \int_{A_m} d\boldsymbol{r}\boldsymbol{t}_m(\boldsymbol{r})\cdot\hat{\boldsymbol{n}}(\boldsymbol{r})\times\boldsymbol{\mathcal{K}}_1\{\boldsymbol{b}_n\}(\boldsymbol{r}) - \int_{A_m} d\boldsymbol{r}\boldsymbol{t}_m(\boldsymbol{r})\cdot\boldsymbol{\mathcal{T}}_1\{\boldsymbol{b}_n\}(\boldsymbol{r}), \quad \text{(A16)}$$

$$Z_{m'n}^{(12,21)} = \frac{\eta_1^{-1}}{2}\int_{A_m} d\boldsymbol{r}\boldsymbol{t}_m(\boldsymbol{r})\cdot\hat{\boldsymbol{n}}(\boldsymbol{r})\times\boldsymbol{b}_n(\boldsymbol{r}) - \eta_1^{-1}\int_{A_m} d\boldsymbol{r}\boldsymbol{t}_m(\boldsymbol{r})\cdot\hat{\boldsymbol{n}}(\boldsymbol{r})\times\boldsymbol{\mathcal{T}}_1\{\boldsymbol{b}_n\}(\boldsymbol{r}) + \eta_1^{-1}\int_{A_m} d\boldsymbol{r}\boldsymbol{t}_m(\boldsymbol{r})\cdot\boldsymbol{\mathcal{K}}_1\{\boldsymbol{b}_n\}(\boldsymbol{r}), \quad \text{(A17)}$$

$$Z_{m'n}^{(21,21)} = -\frac{\eta_1}{2}\int_{A_m} d\boldsymbol{r}\boldsymbol{t}_m(\boldsymbol{r})\cdot\hat{\boldsymbol{n}}(\boldsymbol{r})\times\boldsymbol{b}_n(\boldsymbol{r}) + \eta_1\int_{A_m} d\boldsymbol{r}\boldsymbol{t}_m(\boldsymbol{r})\cdot\hat{\boldsymbol{n}}(\boldsymbol{r})\times\boldsymbol{\mathcal{T}}_1\{\boldsymbol{b}_n\}(\boldsymbol{r}) - \eta_1\int_{A_m} d\boldsymbol{r}\boldsymbol{t}_m(\boldsymbol{r})\cdot\boldsymbol{\mathcal{K}}_1\{\boldsymbol{b}_n\}(\boldsymbol{r}). \quad \text{(A18)}$$

Finally, incident electromagnetic fields are tested only by the RWG functions located on the surface S_{01}, and the elements of the RHS vector for m = 1, 2,. . ., N_{01} are calculated as in (A4) and (A5).

[45] Next, we consider a coated metallic object in homogeneous space. In this case, there are two nonmetallic regions, i.e., D_0 and D_1, and the size of the matrix equation is $(N + N_D) \times (N + N_D)$, where $N_D < N$. Let the

first N_D RWG functions be located on the surface S_{01} and the remaining $N_{12} = (N - N_D)$ RWG functions be located on the metallic surface S_{12}. Then, the expressions for the matrix elements in the diagonal partition $\overline{\boldsymbol{Z}}^{(11)}$ are the same as the expressions in (A7), (A10), (A13), and (A16), which are derived for the coated dielectric object. On the other hand, the off-diagonal partition $\overline{\boldsymbol{Z}}^{(12)}$ becomes a rectangular matrix with two subpartitions, i.e.,

$$\overline{\boldsymbol{Z}}^{(12)} = \begin{bmatrix} \overline{\boldsymbol{Z}}^{(12,11)} \\ \overline{\boldsymbol{Z}}^{(12,21)} \end{bmatrix}_{N \times N_D}, \tag{A19}$$

where the matrix elements $Z_{mn}^{(12,11)}$ and $Z_{m'n}^{(12,21)}$ for m, $n = 1, 2, \ldots, N_D$ and $m' = 1, 2, \ldots, N_{12}$ are calculated as in (A8) and (A17). The off-diagonal partition $\overline{\boldsymbol{Z}}^{(21)}$ also becomes a rectangular matrix, i.e.,

$$\overline{\boldsymbol{Z}}^{(21)} = \left[\overline{\boldsymbol{Z}}^{(21,11)} \overline{\boldsymbol{Z}}^{(21,12)} \right]_{N_D \times N}, \tag{A20}$$

where the subpartitions $Z_{mn}^{(21,11)}$ and $Z_{mn'}^{(21,12)}$ for m, $n = 1, 2, \ldots, N_D$, and $n' = 1, 2, \ldots, N_{12}$ are calculated as in (A9) and (A15). The diagonal partition $\overline{\boldsymbol{Z}}^{(22)}$ is an $N_D \times N_D$ matrix with elements $Z_{mn}^{(22)} = Z_{mn}^{(11)}$ for m, $n = 1, 2, \ldots, N_D$. Finally, the elements of the RHS vector are calculated as in (A4) and (A5) for $m = 1, 2, \ldots, N_D$.

[46] **Acknowledgments.** This work was supported by the Turkish Academy of Sciences in the framework of the Young Scientist Award Program (LG/TUBA-GEBIP/2002-1-12), by the Scientific and Technical Research Council of Turkey (TUBITAK) under research grants 105E172 and 107E136, and by contracts from ASELSAN and SSM.

References

Chang, Y., and R. F. Harrington (1977), A surface formulation for characteristic modes of material bodies, *IEEE Trans. Antennas Propag.*, *25*, 789–795.

Chew, W. C., J.-M. Jin, E. Michielssen, and J. Song (2001), *Fast and Efficient Algorithms in Computational Electromagnetics*, Artech House, Boston, Mass.

Donepudi, K. C., J.-M. Jin, and W. C. Chew (2003), A Higher order multilevel fast multipole algorithm for scattering from mixed conducting/dielectric bodies, *IEEE Trans. Antennas Propag.*, *51*, 2814–2821.

Ergül, Ö., and L. Gürel (2007), Fast and accurate solutions of scattering problems involving dielectric objects with moderate and low contrasts, paper presented at Computational Electromagnetics Workshop, Comput. Electromagn. Res. Cent., Izmir, Turkey.

Ergül, Ö., and L. Gürel (2009), Comparison of integral-equation formulations for the fast and accurate solution of scattering problems involving dielectric objects with the multilevel fast multipole algorithm, *IEEE Trans. Antennas Propag.*, *57*, 176–187.

Ergül, Ö., A. Ünal, and L. Gürel (2007), MLFMA solutions of transmission problems involving realistic metamaterial walls, paper presented at Computational Electromagnetics Workshop, Comput. Electromagn. Res. Cent., Izmir, Turkey.

Fostier, J., and F. Olyslager (2008), An asynchronous parallel MLFMA for scattering at multiple dielectric objects, *IEEE Trans. Antennas Propag.*, *56*, 2346–2355.

Gürel, L., and W. C. Chew (1990), Recursive algorithms for calculating the scattering from N strips or patches, *IEEE Trans. Antennas Propag.*, *38*, 507–515.

Gürel, L., and Ö. Ergül (2003), Comparisons of FMM implementations employing different formulations and iterative solvers, paper presented at Antennas and Propagation Society International Symposium, Inst. of Electr. and Electron Eng., Columbus, Ohio.

Gürel, L., and Ö. Ergül (2006), Extending the applicability of the combined-field integral equation to geometries containing open surfaces, *IEEE Antennas Wireless Propag. Lett.*, *5*, 515–516.

Koc, S., J. Song, and W. C. Chew (1999), Error analysis for the numerical evaluation of the diagonal forms of the scalar spherical addition theorem, *SIAM J. Numer. Anal.*, *36*, 906–921.

Luo, C., and C.-C. Lu (2007), Electromagnetic scattering computation using a hybrid surface and volume integral equation formulation, *ACES J.*, *22*, 340–349.

Poggio, A. J., and E. K. Miller (1973), Integral equation solutions of three-dimensional scattering problems, in *Computer Techniques for Electromagnetics*, edited by R. Mittra, Pergamon, Oxford, U. K.

Rao, S. M., D. R. Wilton, and A. W. Glisson (1982), Electromagnetic scattering by surfaces of arbitrary shape, *IEEE Trans. Antennas Propag.*, *30*, 409–418.

Sheng, X.-Q., J.-M. Jin, J. Song, W. C. Chew, and C.-C. Lu (1998), Solution of combined-field integral equation using multilevel fast multipole algorithm for scattering by homogeneous bodies, *IEEE Trans. Antennas Propag.*, *46*, 1718–1726.

Song, J., C.-C. Lu, and W. C. Chew (1997), Multilevel fast multipole algorithm for electromagnetic scattering by large complex objects, *IEEE Trans. Antennas Propag.*, *45*, 1488–1493.

Ubeda, E., J. M. Rius, and J. Romeu (2006), Preconditioning techniques in the analysis of finite metamaterial slabs, *IEEE Trans. Antennas Propag.*, *54*, 265–268.

Van der Vorst, H. A. (1992), Bi-CGSTAB: A fast and smoothly converging variant of Bi-CG for the solution of nonsymmetric linear systems, *SIAM J. Sci. Stat. Comput.*, *13*, 631–644.

Wu, T. K., and L. L. Tsai (1977), Scattering from arbitrarily shaped lossy dielectric bodies of revolution, *Radio Sci.*, *12*, 709–718.

Ylä-Oijala, P. (2008), Numerical analysis of combined field integral equation formulations for electromagnetic scattering

by dielectric and composite objects, *Prog. Electromagn. Res. C*, *3*, 19–43.

Ylä-Oijala, P., and M. Taskinen (2005a), Application of combined field integral equation for electromagnetic scattering by dielectric and composite objects, *IEEE Trans. Antennas Propag.*, *53*, 1168–1173.

Ylä-Oijala, P., and M. Taskinen (2005b), Well-conditioned Müller formulation for electromagnetic scattering by dielectric objects, *IEEE Trans. Antennas Propag.*, *53*, 3316–3323.

Ylä-Oijala, P., M. Taskinen, and S. Järvenpää (2005a), Surface integral equation formulations for solving electromagnetic scattering problems with iterative methods, *Radio Sci.*, *40*, RS6002, doi:10.1029/2004RS003169.

Ylä-Oijala, P., M. Taskinen, and J. Sarvas (2005b), Surface integral equation method for general composite metallic and dielectric structures with junctions, *Prog. Electromagn. Res.*, *52*, 81–108.

Ylä-Oijala, P., M. Taskinen, and S. Järvenpää (2008), Analysis of surface integral equations in electromagnetic scattering and radiation problems, *Eng. Anal. Boundary Elem.*, *32*, 196–209.

Ö. Ergül and L. Gürel, Department of Electrical and Electronics Engineering, Bilkent University, Bilkent, TR-06800 Ankara, Turkey. (ergul@ee.bilkent.edu.tr; lgurel@bilkent.edu.tr)